MNRAS **000**, 000–000 (0000) Preprint 19 February 2018 Compiled using MNRAS LATEX style file v3.0

We are not the 99 percent: quantifying asphericity in the distribution of Local Group satellites

Jaime E. Forero-Romero [1] ⋆, Verónica Arias[1]
[1] *Departamento de Física, Universidad de los Andes, Cra. 1 No. 18A-10 Edificio Ip, CP 111711, Bogotá, Colombia*

19 February 2018

ABSTRACT
We use numerical simulations to build an explicit probability distribution for the asphericity in the satellite distribution around galaxies similar to the Local Group (LG) in the Lambda Cold Dark Matter (LCDM) paradigm. This allows us to estimate the atipicallity of the satellite distributions in the LG even when the underlying simulations do not have enough systems that fully resemble the LG. We demonstrate the method using three different simulations: Illustris-1, Illustris-1-Dark and ELVIS. Detailed results differ among the simulations suggesting a strong influence of the typical Dark Matter (DM) halo mass in the LG samples. However, there are three common trends. First, at most of 2% the pairs are expected to have satellite distributions with the same asphericity as the LG; second, between 27% to 56% of the pairs have a halo with a satellite distribution as aspherical as in M31; and third, at most 3% of the pairs have a satellite distribution as planar as in the MW. The brightest satellites in the M31 galaxy have a rather typical distribution in the LCDM context, while the MW distribution is atypical in this respect. These results place the LG at the level of a 3σ outlier in the LCDM paradigm. We suggest that to understand this atipicality will require quantifying the probability distribution for the satellite distribuition asphericity as a function of halo mass and large scale environment. The approach presented here can facilitate that study and other comparisons between different numerical setups and choices to study satellites around LG pairs in simulations.

Key words: Galaxies: halos — Galaxies: statistics — Dark Matter — Methods: numerical

1 INTRODUCTION

The spatial distribution of satellite galaxies around our Milky Way (MW) and the M31 galaxy provides a stringent test for structure formation theories in a explicit cosmological context (Pawlowski et al. 2015; Sawala et al. 2016). The presence of a Vast Polar Structure of satellites around the Milky Way, first suggested by Kunkel & Demers (1976) and Lynden-Bell (1976) as a Magellanic Plane, has been stablished in the last decade (Kroupa et al. 2005; Pawlowski et al. 2013). This structure is present in the 11 brightest "classical" dwarf galaxies and has been confirmed as fainter satellites have been detected (Belokurov et al. 2014). In the case of M31, observational studies have found a planar satellite distribution in a subset of 15 satellites out of the total poulation of 27 satellites.(Conn et al. 2013; Ibata et al. 2013), although its brightest satellites do not show any special feature and are consistent with a random distribution (Koch & Grebel 2006; Metz et al. 2007).

The question whether this kind of planar configurations are atypical on cosmological samples has not been properly addressed given the current observational limitations. For instance, comparisons in large galaxy surveys have only been able to constrain that 5% of the Milky-Way like galaxies in the Universe have two bright satellite galaxies as is the case of the Milky Way and its Large and Small Magellanic Clouds (Liu et al. 2011), or that pairs of bright satellites preferentially show anti-correlated when they are diametrically oposed (Ibata et al. 2014). A planar structure outside the Local Group (LG) has been confirmed in Centaurus A (Müller et al. 2018) a galaxy that is only $\sim$ 4Mpc away.

To date, the atipicallity of satellite distributions can only be addressed in simulations. First studies Most of the studies have been performed in the currently preferred paradigm, which is based on a Cold Dark Matter cosmology in a expanding Universe described by General Relativity including a Cosmological Constant, the so-called Lambda

⋆ je.forero@uniandes.edu.co

Cold Dark Matter (LCDM) model. The broad consensus is that these highly structured satellite distributions are hard to find in simulations (). There are still disagreements on the precise degree of atypicallity and the conditions required to simulate satellite distributions closer. These disagreements seem to be originated on what is considered to be a LG analog in the simulation.

Some studies have focused on the individual dark matter halos that could host galaxies like the MW or M31, while some other studies have tried to simulate the formation of galaxy pairs resembling both the MW and M31. The transition from individual halos to pairs has been motivated by studies that show how the LG location in the cosmic web plays a role in distinguishing the MW and M31 halos from the average $\sim 10^{12}$ $M_\odot$ DM halo (Forero-Romero et al. 2011) Studies of the LG as a pair of isolated DM halos have also found that the LG itself has relatively atypical kinematics in the context of LCDM and a strong preference to lie along filaments (Forero-Romero et al. 2013). Putting together these pieces, the cosmic web should therefore play a determinant role in building up planar satellite distributions through preferential alignments and accretions histories of galaxies (Forero-Romero et al. 2014).

The aim of our work is to overcome two difficulties in the study of atipicallity in satellite distributions. First, atypicallity is usually computed from distributions comming from different simulated pair samples, making it inconvenient to compare results from different studies. Second, halo pairs similar to the LG are scarse in cosmological volumes, making it hard to perform direct comparisons against simulated systems that fully resemble the LG.

We surmount the first difficulty by setting as a point of reference a spherical satellite distribution and not LCDM simulations. This spherical distribution is built from the data itself (observational or simulated) by randomizing its angular position around the central galaxy and keeping its radial distance fixed (Pawlowski et al. 2017). We characterize each satellite distribution with its inertia tensor and summarize the results with the scalars describing the width of the distribution and its axis ratios.

We handle the second difficuly by building an explicit analytic probability distribution that is compatible with the simulated data. We then use the simulations to estimate the parameters in this distribution to later use it as a parent sample to generate any desired number of samples that are by construction statistically compatible with simulations.

To summarize, simulations help us first to construct an explicit probability distribution for deviations from sphericity for a given LCDM simulated sample and then, using this distribution, we compute the odds of finding a satellite distribution that deviates from sphericity as much as the LG does.

In Section 2 we list the sources of the observational and simulated data to be used throughout the paper. In Section 3 we describe the methods we use to build halo pairs and characterize its satellite distributions. In Section 4 we present our results to finally conclude in Section 5.

2 DATA SAMPLES

2.1 Observational Data

The base for our analysis is the catalog compiled in (Pawlowski et al. 2014) which reports information on all galaxies within 3 Mpc around the Sun to that date. Detailed description of the compiled catalog can be found in (Pawlowski et al. 2013), here we summarize the relevant features for the current study.

The information in the catalogue is based on the catalogue compiled by McConnachie (2012). The distance estimates are based on resolved stellar populations. We use three dimensional positions in a cartesian coordinate system as computed by Pawlowski et al. (2013). In this coordinate system the z-axis points towards the Galactic north pole, the x-axis points in the direction from the Sun to the Galactic centre, and the y-axis points in the direction of the Galactic rotation.

For both the M31 and MW we only use the 11 to 15 brightest satellites (using M_V magnitudes) within a distance of 300kpc to its central galaxy. The satellites included for the MW analysis are: LMC, SMC, Canis Major, Sagittarius dSph, Fornax, Leo I, Sculptor, Leo II, Sextans I, Carina, Ursa Minor, Draco, Canes Venatici (I), Hercules and Bootes II. The satellites included for the M31 analysis are: Triangulum, NGC205, M32, IC10, NGC185, NGC147, Andromeda VII, Andromeda II, Andromeda XXXII, Andromeda XXXI, Andromeda I, Andromeda VI, Andromeda XXIII, LGS 3, and Andromeda III.

2.2 Data from the Illustris project

We use publicly available data from the Illustris Project (Vogelsberger et al. 2014). This suite of cosmological simulations, performed using the quasi-Lagrangian code AREPO (Springel 2010), followed the coupled evolution of dark matter and gas and includes parametrizations to account for the effects of gas cooling, photoionization, star formation, stellar feedback, black hole and super massive black hole feedback. The simulation volume is a cubic box of 75 $\mathrm{Mpc}\,h^{-1}$ on a side. The cosmological parameters correspond to a ΛCDM cosmology consistent with WMAP-9 measurements (Hinshaw et al. 2013).

We extract halo and galaxy information from the Illustris-1 and Illustris-1-Dark simulations, the former simulation includes hydrodynamics and star formation prescriptions while the latter only includes dark matter physics. These simulations have the highest resolution in the current release of the Illustris Project. Illustris-1 has 1820^3 dark matter particles and 1820^3 initial gas volumen elements, while Illustris-1-Dark has 1820^3 dark matter particles. This corresponds to a dark matter particle mass of $6.3 \times 10^6 M_\odot$ and a minimum mass for the baryonic volume element of $8.0 \times 10^7 M_\odot$for Illustris-1 and a dark matter particle mass of $7.6 \times 10^6 M_\odot$for Illustris-1-Dark. In both simulations the dark matter gravitational softening is 1.4 kpc.

We buid a sample of pairs that resemble the conditions in the LG. To construct this sample we select from Illustris-1 all galaxies with a stellar mass in the range $1 \times 10^{10} M_\odot < M_\star < 1.5 \times 10^{11} M_\odot$. Then we select the pairs with the following conditions.

Reference	Target Measurement	Parent Sample	Probability (%)
Kroupa et al. (2005)	RMS height in MW's 11 classical satellites	Monte Carlo from an spherical power law radial distribution.	< 0.5
Libeskind et al. (2005)	Triaxiality of MW's 11 classical satellites	6 high resolution DM only N-body simulations.	common
Zentner et al. (2005)	Triaxiality and disk height in MW's 11 classical satellites	3 high resolution DM only N-body simulations.	2
Koch & Grebel (2006)	RMS height in M31's 15 brightest satellites	Monte Carlo satellite distributions with a power law radial distribution	$87 - 99$
Metz et al. (2007)	Triaxiality and RMS height in MW's 11-13 brightest satellites	Monte Carlo from a halo triaxiality distribution from LCDM simulations	< 0.5
Metz et al. (2007)	Triaxiality and RMS height in M31's 16 brightest satellites	Monte Carlo from an spherical power law radial distribution	17

Table 1. Probability results derived in previous publications.

- For each galaxy A we find its closest galaxy B, if galaxy A is also the closest to halo B, the two are considered as a pair.
- With d_{AB} the distance between the two galaxies and $M_{\star,min}$ the lowest stellar mass in the two galaxies, we discard pairs that have any other galaxy C with stellar mass $M_\star > M_{\star,min}$ closer than $3 \times d_{AB}$ from any of the pair's members.
- The distance d_{AB} is greater than 700 kpc.
- The relative radial velocity between the two galaxies, including the Hubble flow, is -120 km s^{-1} $< v_{AB,r} <$ 0 km s^{-1}.

We find 27 pairs with these conditions. We then select the pairs where in both halos there are at least 15 detected subhalos, thus discarding pairs with halos with the lowest mass. We end up with a total of 20 pairs in Illustris-1. In Illustris-1-DM we use the center of mass position of the 27 pairs in Illustris-1 to find the matching halo pairs. After discarding the pairs with less than 15 detected subhalos in one of the halos we end up with a total of 24 pairs. This corresponds to a pair number density of $\sim 2 \times 10^{-5}$ pairs Mpc^{-3} Appendix A shows the physical properties (stellar masses, maximum circular velocities, radial velocities and separation) of those pairs.

Although Illustris-1 has stellar particles, we do not use their properties to select the satelite population because the smallest galaxies are barely resolved in stellar mass at magnitudes of $M_V = -9$, close to the limit of the 11 "classical" MW satellites. We use instead the dark matter information as the smallest sub-halos we care about are sampled with at least 40 particles.

Both in Illustris-1 and Illustris-1-DM we chose the satellite samples by ranking the subhalos in decreasing order of its current maximum circular velocity and select the first N_p halos in the list. The results presented here correspond to $11 \leq N_p \leq 15$.

2.3 Data from the ELVIS project

We use data from the public release of the Exploring the Local Universe In Simulations (ELVIS) project. For a detailed description of that project and its data we refer the reader to Garrison-Kimmel et al. (2014). Here we summarize the elements relevant to our discussion.

ELVIS data comes from resimulations of dark matter halo pairs selected in dark matter only cosmological simulations. The parent cosmological boxes have a cosmology consistent with the Wilkinson Microwave Anisotropy Probe 7 results.

The ELVIS project used the results from 50 simulation boxes of side lenght 70.4 Mpc to select pairs with kinematic characteristics similar to the LG. These selection criteria included the following

- The virial mass of each host must be in the range $1 \times 10^{12} M_\odot < M_{vir} < 3 \times 10^{12} M_\odot$
- The total pair mass must be in the range $2 \times 10^{12} M_\odot < M_{vir} < 5 \times 10^{12} M_\odot$
- The center of mass separation is in the range $0.6 \leq d \leq 1$ Mpc.
- The relative radial velocity is negative.
- No halos more massive than the least massive halo within 2.8 Mpc and no halos with $M_{vir} > 7 \times 10^{13}$ within 7 Mpc of the pairs' center of mass.

This corresponds to a pair number density of $\sim 8 \times 10^{-6}$ pairs Mpc^{-3}, this is a factor ~ 2.5 lower than the pair number density we find in the Illustris data. There were a total of 146 pairs that met those criteria, but only 12 were chosen for resimulation. Additionally, the selected pairs for resimulation have a relative tangential velocity less than 75km s^{-1}. The dark matter particle resolution in these resimulations is 1.9×10^5, a thousand times larger than Illustris-1. In this paper we only use the results from these 12 resimulated pairs.

Appendix A compares the physical properties (stellar masses, maximum circular velocities, radial velocities and separation) in those pairs against the results from the Illustris-1 simulations.

3 BUILDING, CHARACTERIZING AND COMPARING SATELLITES SPATIAL DISTRIBUTIONS

3.1 Building Satellite Samples

We compare the joint satellite distributions in the MW and M31 at fixed satellite number, N_s. This means that the magnitude cut corresponding to the faintest satellite included in the sample is different in each case. We make this choice for two reasons. First, to be sure that there is a non-zero number of satellites in the simulations to make the computations. Second, to rule out the influence of satellite numbers in the statistics.

We compute the satellite statistics for 11 up to 15 satellites. The lower limit corresponds to the number of classical Milky Way satellites. The upper limit corresponds to the maximum number of satellites that can be resolved in both halos for most of the isolated pairs in Illustris-1. In simulations we rank the subhalos by their maximum circular velocity, in observations we rank the satellites by its M_V magnitude.

We also use two kinds of satellite distributions. The first keeps the positions for the satellites fixed as provided in the observations/simulations; the second randomizes the angular positions of the satellites around the central galaxy while keeping its radial distance fixed. The randomization process is done 1000 times for each galaxy.

3.2 Describing Samples with the Inertia Tensor

We base all our results on the description provided by the inertia tensor defined by the satellites' positions.

$$\overline{\mathbf{I}} = \sum_{k=1}^{N_s} [(\mathbf{r_i} - \mathbf{r_0})^{\mathbf{2}} \cdot \mathbf{1} - (\mathbf{r_i} - \mathbf{r_0}) \cdot (\mathbf{r_i} - \mathbf{r_0})^{\mathbf{T}}], \quad (1)$$

where k indexes the set of satellites of interest $\mathbf{r_k}$ are the satellites' positions, $\mathbf{r_0}$ is the location of the central galaxy $\mathbf{1}$ is the unit matrix, and $\mathbf{r}^T$ is the transposed vector $\mathbf{r}$. We use $\mathbf{r_0}$ as the position of the central galaxy, and not the satellites' geometrical center, to allow for a fair comparison once the angular positions of the satellites are randomized around this point.

From this tensor we compute its eigenvalues, $\lambda_1 > \lambda_2 > \lambda_3$, and corresponding eigenvectors, $\hat{I}_1$, $\hat{I}_2$, $\hat{I}_3$. We define the size of the three ellipsoidal axis as $a = \lambda_1$, $b = \lambda_2$ and $c = \lambda_3$. We also define $\hat{n} \equiv \hat{I}_1$ as the vector perpendicular to the planar satellite distribution. We also define the width, w, of the planar satellite distribution, as the standard deviation of all satellite distances to the plane defined by the vector $\hat{n}$.

To summarize we characterize the satellite distribution by for quantities obtained from the inertia tensor:

- Plane width, w.
- c/a axis ratio.
- b/a axis ratio.

3.3 Comparing Satellite Samples

We compare every satellite distribution against its own spherically randomized distribution. We keep fixed the radial position of every satellite with respect to the central galaxy and then randomize its angular position. We repeat this procedure 1000 times for each satellite distribution and proceed to measure the quantities mentioned in the previous section: w, c/a and b/a. For each quantity we compute the average and standard deviation from the 1000 random samples. This allows us to build a normalized version of all quantities of interest by substracting the mean and dividing between the standard deviation of the randomized samples.

This allows us to make a first comparison. The observed/simulated distribution against its randomized version. The second intermediate comparison we make is of the observations against the simulations. The final comparison is between the normalized quantities, both observed and simulated.

The comparison between the normalized quantities is the one that carries the important information about the deviations from spheriticy. We do not want to directly compare how the observations deviate from simulations but to compare the deviations from asphericity in observations and simulations.

3.4 Describing joint satellite distributions

After building the normalized variables with the simulated data we perform a Kolmogorov-Smirnov test with the null hypothesis of belonging to a normal distribution with mean and standard deviation computed from the mean and standard deviation from the data itself. We find that the distributions for the normalized w, c/a and b/a are consistent with gaussian ditributions.

Based on this result we build a multivariate normal distribution for the joint distributions of the normalized w, c/a and b/a:

$$p(X; \mu, \Sigma) = \frac{1}{(2\pi)^{3/2}|\Sigma|^{1/2}} \exp\left(-\frac{1}{2}(X-\mu)^T \Sigma^{-1} (X-\mu)\right), \quad (2)$$

where $X = [w, c/a, b/a]^T$ is a vector variable with the normalized quantities, μ is the vector mean and the Σ is the covariance matrix.

We compute the preferred covariance matrix and the mean distribution values with a jackknife technique. That is, out of the the n pairs we have, we perfom n different covariance and mean value measurements using only $n-1$ pairs. The reported covariance and mean values correspond to the average of all measurements, the corresponding standard deviation also helps us to estimate the uncertainty on every reported coefficient. This compact description allows us to generate samples of size N that are consistent by construction with their parent simulation.

Finally, we use the generated samples to estimate how common are the deviations from sphericity that we measure in the observational data. We use a double-tailed test in this comparison, meaning that we always measure the fraction of points with absolute values larger than the treshold absolute observed value.

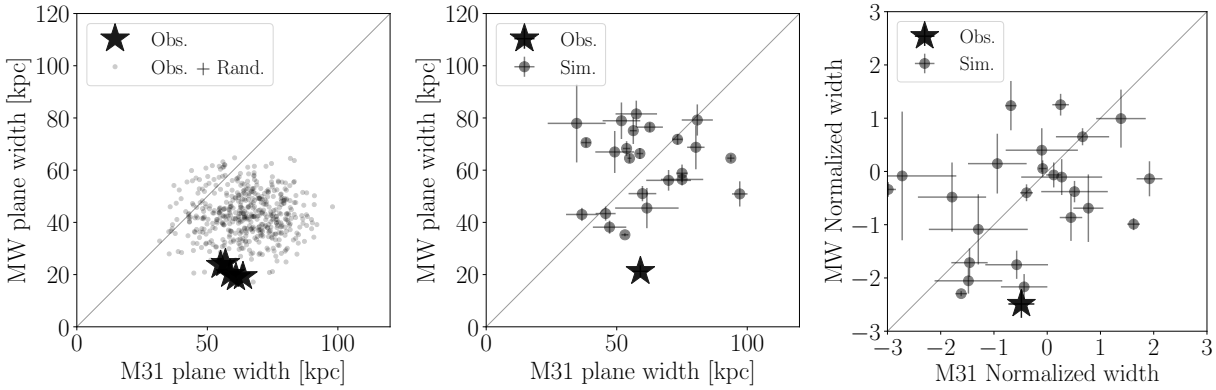

Figure 1. Plane width characterization in observations and simulations (Illustris1-Dark in this case). In all panels the horizontal/vertical axis corresponds to the M31/MW or the most/less massive halo in the pair Left. Plane width in physical units comparing the results from observations (stars) against the result of spherically randomizing the satellite positions (circles). Middle. Average from the observations (star) and the average from each pair in the simulation (circles). Right. Same as the middle panel except that this time each point has been normalized (median substracted and normalized by the standard deviation) to the results of its randomization. The main message of these panels is that the MW has a significantly thinner plane both compared to the result of its own satellite spherical randomization (left panel) and the expectation from simulations (middle and right panel). This low value is 2σ away from what is expected in a spherical distribution. In M31 the satellite distribution is in agreement with the expectations both from an spherical distribution and the results form the simulations.

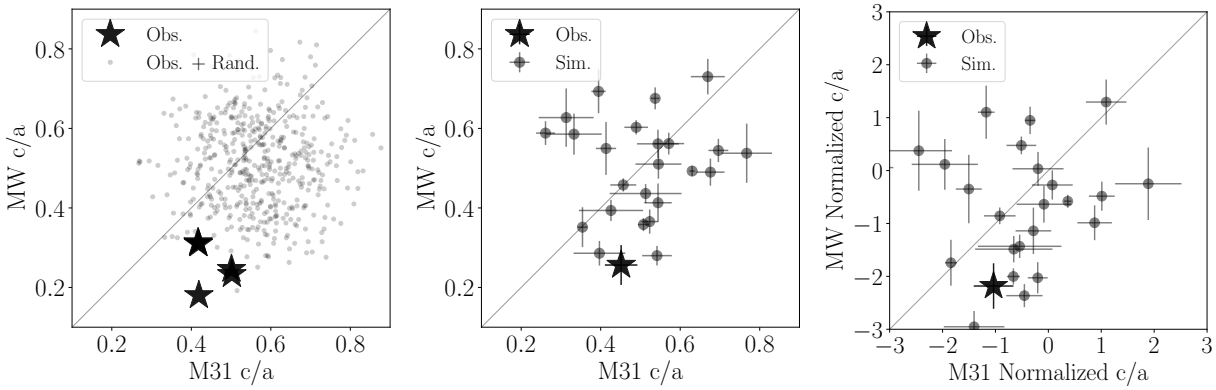

Figure 2. Same layout as in Figure 1. This time for the c/a axis ratio. The same message holds in this case; namely, that the MW has a significantly lower c/a value than the expectation from the spherical distribution and from the simulations. This low value is also 2σ away from the expactations for a spherical distribution. On the other hand, M31 is consistent both with a spherical distribution and with the results from simulations.

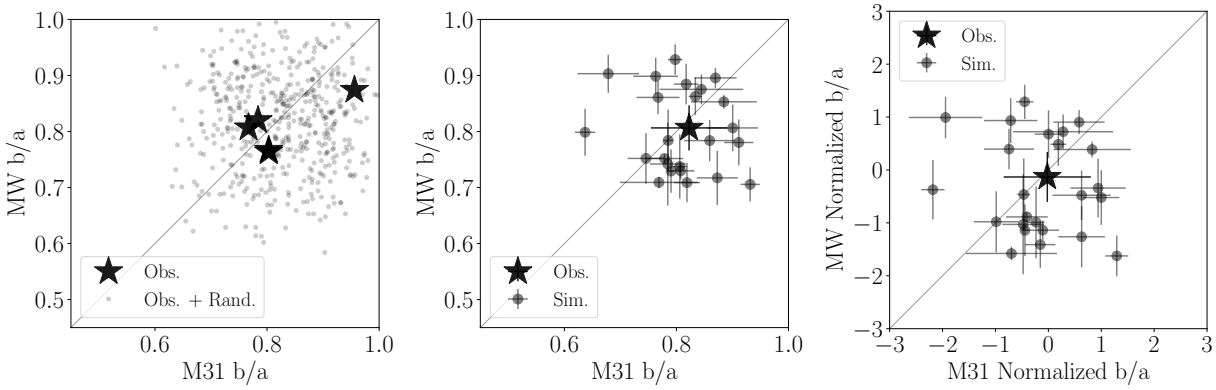

Figure 3. Same layout as in Figure 1. This time for the b/a axis ratio. In this case both the MW and M31 are consistent with the results of a spherical distribution and the simulations.

	Observations		Randomized Obs.		Normalized Units	
	M31	**MW**	**M31**	**MW**	**M31**	**MW**
Plane width (kpc)	59 ± 3	21 ± 2	65 ± 12	45 ± 8	-0.48 ± 0.24	-2.48 ± 0.26
c/a ratio	0.45 ± 0.04	0.25 ± 0.05	0.55 ± 0.10	0.53 ± 0.10	-1.03 ± 0.37	-2.18 ± 0.42
b/a ratio	0.82 ± 0.06	0.80 ± 0.04	0.82 ± 0.07	0.81 ± 0.08	-0.02 ± 0.82	-0.13 ± 0.47

Table 2. Results from observations. Mean values and standard deviations for the different quantities describing the satellite distributions: plane width, c/a ratio and b/a ratio. The first colum refers to the results from observational data, the second column uses the spherically randomized version of the observational data, the third column corresponds to the observational data recentered and normalized by the randomized values.

	Illustris-1-Dark		Illustris-1		ELVIS	
	M31	**MW**	**M31**	**MW**	**M31**	**MW**
Plane width (kpc)	62 ± 3	61 ± 3	70 ± 4	67 ± 2	70 ± 2	68 ± 4
c/a ratio	0.50 ± 0.01	0.50 ± 0.02	0.52 ± 0.01	0.53 ± 0.01	0.54 ± 0.01	0.49 ± 0.02
b/a ratio	0.79 ± 0.01	0.81 ± 0.02	0.80 ± 0.01	0.80 ± 0.02	0.80 ± 0.01	0.81 ± 0.01

Table 3. Results from simulations. Mean values and standard deviations for the different quantities describing the satellite distributions: plane width, c/a ratio and b/a ratio. The first column summarize the results from the 24 pairs in Illustris-1-Dark, the second column from the 20 pairs in Illustris-1 and the third column from the 12 pairs in the ELVIS project.

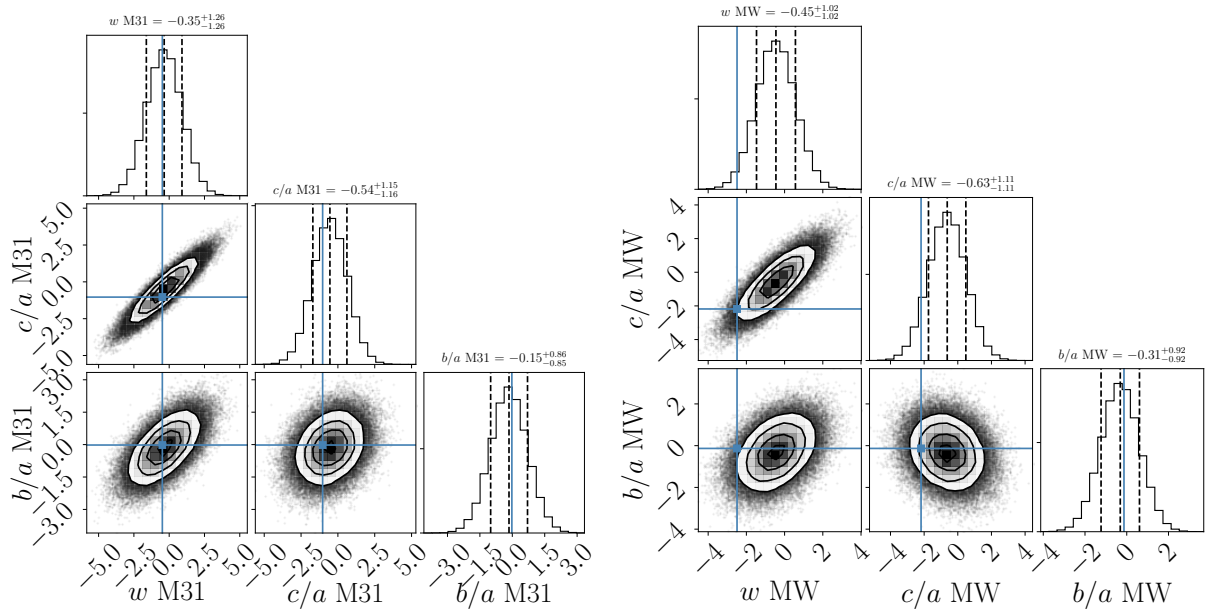

Figure 4. Results from multivariate gaussian model fitted to the normalized values for the plane width w, c/a ratio and b/a ratio from the Illustris1-Dark results. Left/right panel correspond to M31/MW respectively. The cross indicates the observed values. The contour levels in the 2D histograms correspond to the 1σ, 2σ and 3σ contours in two dimensions. The dashed vertical lines in the histograms along the diagonal correspond to the 1σ boundaries in one dimension. The results for the gaussian model are built from 10^6 point realizations in the three-dimensional space spaned by the variables of interest for each halo. This plot clearly shows how the M31 results are well within the expectations from simulations while the MW has an unusual low value for the plane width and the c/a axis ratio.

4 RESULTS

Table 2 and Table 3 summarize the mean values and uncertainties for the plane w, c/a ratio and b/a ratio in the observations and simulations, respectively. The uncertainty in the observations is computed from the results with different number of satellites, while in the simulations it corresponds to the standard deviation over different halos.

The observed widths are always smaller than its randomized version. For M31 there is barely a ratio of 0.92 between observed and randomized, while for the MW this

factor goes down to less than half 0.48. The observed c/a ratio follows the same extreme trend for the MW compared to a M31 distribution closer to spherical, The b/a ratio is statisically the same between observations and the spherical randomization.

In the following subsections we describe in detail the results on the distributions for w, c/a and b/a. The plots in the main body of the paper correspond to the Illustris1-Dark simulation; the results from the other simulations are included in the Appendix.

4.1 Plane Width

Figure 1 summarizes the results for the width measurements. The left panel compares the results for the MW and M31 observations (stars) against its spherically randomized satellites (circles). The most interesting outcome is that the MW plane width is smaller than $\approx 98\%$ of the planes computed from the randomized distribution, while the M31 plane width is only slightly smaller than the average of the distribution.

The middle panel in Figure 1 compares the observational result (star) against the measurements of all pairs from the Illustris1-Dark simulation (circles). In this case we have a similar result as before. The observed MW width is smaller than all the results in the simulation, there is not a single halo with similar values. On the other hand, the results for the M31 are entirely consistent with observations. Most of the halos in the simulation show a width value similar to M31.

The right panel in Figure 1 shows the result for the normalized width. This panel tells the same story as the middle panel. The M31 values are typical while the MW is an outlier. The added value of the data in this panel is that it is the normalized which is consistent with normal distributions. This is the data used to build the mean values vector and covariance matrix described in Equation **??**

4.2 c/a axis ratio

Figure 2 shows the results for the minor to major axis ratio. The layout is the same as in Figure 1. The results for the c/a ratio follow the same trends as for the width w.

The left panel in Figure 2 shows how the MW c/a ratio is significantly lower than the measured values for spherical distributions, and it is smaller than $\approx 98\%$ of the randomized distributions. On the other hand the ratio for M31 is lower than the mean of the spherical values but still well within its variance. The middle panel in the same Figure shows the LG compared against the results in the simulations. In this case we find a similar trend as before. The MW is atypical and M31 is within the variance from the simulation data. This time, however, there are two MW-like halos out of the total of 24 that show an c/a as small as that of the MW. The right panel shows the normalized results. The MW shows a low c/a ratio close to between two and three standard deviations away from the mean value of the spherical distribution; this contrasts with the results for M31 which are close to 1 standard deviation away.

4.3 b/a axis ratio

Figure 3 shows the results for the minor to major axis ratio with the same layout as Figure **??** In all cases of comparison (against randomized distribution and simulations) the results for both the MW and M31 are typical.

4.4 Fit to a Multivariate Gaussian Distributions

Figure 4 illustrates the results from computing the covariance matrix and mean vector in Eq.2 from the normalized quantities obtained from the Illlustris1-Dark simulation. The distributions in this Figure are computed from 10^6 with the multivariate gaussian. Similar plots for Illustris1 and ELVIS are in the Appendix. The values for all the covariance matrices and mean vectors foricorresponding to all the simulations are listed in the Appendix.

This result nicely summarizes the results we had in the previous sections. The left triangular plot shows how M31 falls into the middle of all 2D distributions and is always close to the peak and within the $1-\sigma$ range. The right plot clearly places the MW observations outside the 3σ range in the joint distributions that involve the width w.

In both cases the strongest positive correlation is present for the width and the c/a axis ratio. A weaker but still positive correlation is present for the width and the b/a axis ratio.

4.5 Number of Expected LG Systems

We use the fits to the multivariate gaussian distributions to compute the expected number of pairs with characteristics similar to those of the LG. To do this we generate 10^3 samples, each sample containing 10^4 pairs, where each pair member is drawn from the corresponding multivariate gaussian distribution.

We consider that a sampled system is similar to the M31/MW galaxy if the distance of each of its characteristics (w, c/a, b/a) to the sample mean is equal or larger than the distance of the observational values to the sample mean. That is, we perform a double-tailed test using the observational values as a threshold.

Figure 5 summarizes the results from this experiment. The left panel shows the probability density for the number of M31 systems in a parent sampe of 10^4 pairs, the right panel shows the results for the MW. For M31, between 27% and 56% of the pairs have a satellite distribution as aspherical as the observed in M31. This fraction drops dramatically for the MW where only 0.02% to 3% of the satellites are expected to have as extreme aspherical distributions as the MW.

Considering the joint distribution of M31 and MW we find that at most 2% of the pairs are expected to be similar to the LG. In a three dimensional gaussian distribution, having a 1σ, 2σ and 3σ interval corresponds to have respectively 19%, 73% and 97% of the total of points in the distribution. With this result in mind the *LG* has the same degree of atipicality as a 3σ outlier.

Among the three simulations, the results infered from ELVIS data show the lowest fraction of M31 and MW systems; for Illustris1-Dark we have the highest fraction of

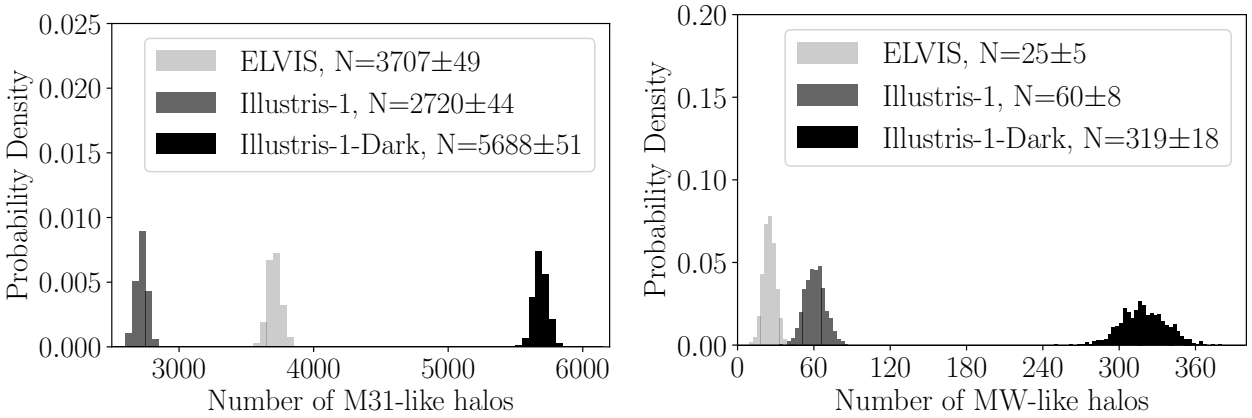

Figure 5. Probability distribution for the expected number of M31 and MW halos showing the same degree of atipicality as the Local Group if drawn from a sample of 10000 isolated pairs. The distributions correspond to results derived from Illustris-DM, Illustris, and ELVIS data. In the most optimistic case (Illustris-DM), 1% of the pairs have two halos with properties similar to the LG. In the case of Illustris this percentage drops to 0.1% and 0.01% for ELVIS.

M31/MW systems. The results from Illustris1 are in between these two, but closer to ELVIS.

The most probable reason for these trends is the different median mass for the MW/M31 halos in the pairs from these simulations. For instance for the MW halo the median maximum circular velocity is ~ 160 km s^{-1}, ~ 150 km s^{-1}and ~ 120 km s^{-1}in the ELVIS, Illustris1 and Illustris1-Dark simulations, respectively. For the M31 halo this median velocity is $\sim$ 200km s^{-1}both for the ELVIS and Illustris1 simulations, while for the Illustris1-Dark it is ~ 160 km s^{-1}.

5 CONCLUSIONS

In this paper we develop and demostrate a method to quantify the asphericity of the satellite distribution in the around the MW and M31. In the interest of keeping the method straightforward and robust we do not look for planes in subsets of satellites or coherent kinematical structures. We focus on the asphericity estimates for a fixed number of the brightest satellites around each galaxy.

The method uses as a reference the spherically randomized data of the system under study (Pawlowski et al. 2017). To this end, we first measure the width and axis ratios for the satellite distributions of interest. Then, we measure the same quantities for the same set of points after a process of spherical randomization. Finally, we renormalize the initial results to the mean value and standard deviation computed from the randomized data.

We find that these normalized quantities are well described by a multivariate gaussian distribution. We fit estimate the mean and covariance of this distributions using the results of LG pairs coming from three different numerical simulations, we inally compare the observational results against the distributions derived from the simulations: Illustris-1, Illustris-1-Dark and ELVIS.

We find that in the best case (Illustris1-DarkMatter) the deviation from asphericity in the observed LG is only expected in 3 ± 2 pairs out of a sample of 10^4 isolated pairs. This places the LG as a 3σ outlier. The weight to explain this atypical result is not distributed equally between the MW and M31. While M31 presents a fully typical asphericity in the expectations from LCDM, the MW shows aspherical deviations in plane width and the major-to-minor axis ratio highly atypical in the framework of LCDM. We estimate that with the M31 between 37% and 58% of the pairs pairs show normalized characteristics larger than M31, while this fraction drops to less than 1% for the MW. These fractions are robust to changes in the numerical simulations and to the criteria used to define the pairs.

The highly aspherical distribution of the brightest MW satellites is in stark contrast to the more spherical M31 distribution. Furthermore, the atipicallity of the MW distribution in the LCDM context adds up to the also atypical presence of two bright satellite galaxies.

The focus of our approach is building explicit probability distributions for the observables of interest, instead of trying to find simulated objects that fulfill different observational criteria. This approach is particularly useful in the case of atypical observables. Building the probability distribution allows for an atypicallity quantification without needing to build explicit samples of objects that are already scarce and difficult to find in simulations.

An extension of this framework to outliers in higher order deviations (i.e. a *subset* of satellites that are in a plane or coherent *velocity* structures) should also be possible, similar to the work presented by XXIbata et al. (2013) on the satellite velocity anisotropy.

From the results we derive in this paper we also estimate that a cosmological volume of at least $(XX)^3$ is required to find a halo pair that shows similar asphericity characteristics as the LG. This atypical satellite distribution should be seen as an opportunity to constrain in high detail the initial conditions and environment that allowed such a pattern to emerge.

ACKNOWLEDGEMENTS

We acknowledge Universidad de los Andes and COLCIENCIAS (Project - XXX) for the computing resources used in this project.

REFERENCES

Belokurov V., Irwin M. J., Koposov S. E., Evans N. W., Gonzalez-Solares E., Metcalfe N., Shanks T., 2014, MNRAS, 441, 2124
Conn A. R., et al., 2013, ApJ, 766, 120
Forero-Romero J. E., Hoffman Y., Yepes G., Gottlöber S., Piontek R., Klypin A., Steinmetz M., 2011, MNRAS, 417, 1434
Forero-Romero J. E., Hoffman Y., Bustamante S., Gottlöber S., Yepes G., 2013, ApJ, 767, L5
Forero-Romero J. E., Contreras S., Padilla N., 2014, MNRAS, 443, 1090
Garrison-Kimmel S., Boylan-Kolchin M., Bullock J. S., Lee K., 2014, MNRAS, 438, 2578
Hinshaw G., et al., 2013, ApJS, 208, 19
Ibata R. A., et al., 2013, Nature, 493, 62
Ibata N. G., Ibata R. A., Famaey B., Lewis G. F., 2014, Nature, 511, 563
Koch A., Grebel E. K., 2006, AJ, 131, 1405
Kroupa P., Theis C., Boily C. M., 2005, A&A, 431, 517
Kunkel W. E., Demers S., 1976, in Dickens R. J., Perry J. E., Smith F. G., King I. R., eds, Royal Greenwich Observatory Bulletins Vol. 182, The Galaxy and the Local Group. p. 241
Libeskind N. I., Frenk C. S., Cole S., Helly J. C., Jenkins A., Navarro J. F., Power C., 2005, MNRAS, 363, 146
Liu L., Gerke B. F., Wechsler R. H., Behroozi P. S., Busha M. T., 2011, ApJ, 733, 62
Lynden-Bell D., 1976, MNRAS, 174, 695
McConnachie A. W., 2012, AJ, 144, 4
Metz M., Kroupa P., Jerjen H., 2007, MNRAS, 374, 1125
Müller O., Pawlowski M. S., Jerjen H., Lelli F., 2018, Science, 359, 534
Pawlowski M. S., Kroupa P., Jerjen H., 2013, MNRAS, 435, 1928
Pawlowski M. S., Kroupa P., Jerjen H., 2014, VizieR Online Data Catalog, 743
Pawlowski M. S., Famaey B., Merritt D., Kroupa P., 2015, ApJ, 815, 19
Pawlowski M. S., et al., 2017, Astronomische Nachrichten, 338, 854
Sawala T., et al., 2016, MNRAS, 457, 1931
Springel V., 2010, MNRAS, 401, 791
Vogelsberger M., et al., 2014, MNRAS, 444, 1518
Zentner A. R., Kravtsov A. V., Gnedin O. Y., Klypin A. A., 2005, ApJ, 629, 219

APPENDIX A: PHYSICAL CHARACTERISTICS OF THE ISOLATED PAIRS SAMPLES

APPENDIX B: RESULTS FROM ELVIS AND ILLUSTRIS1

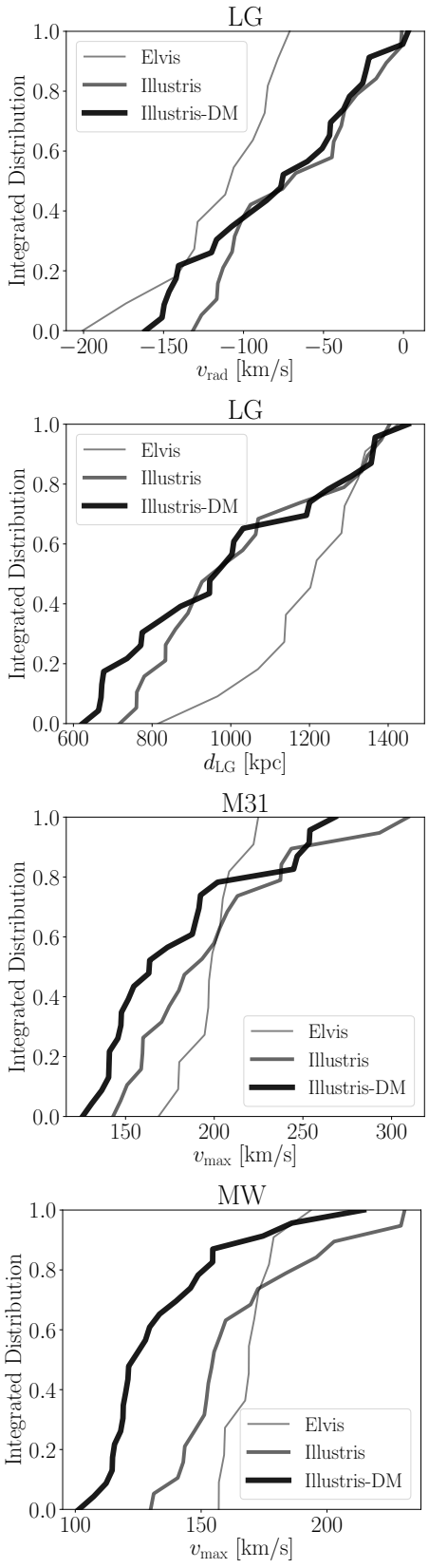

Figure A1. Physical characteristics of the LG pairs selected in the simulations. All lots show the integrated distributions. The physical properties are the radial comoving velocity between the MW and M31, the radial separation between the MW and M31 and the maximum circular velocity for the M31 and MW dark matter halo.

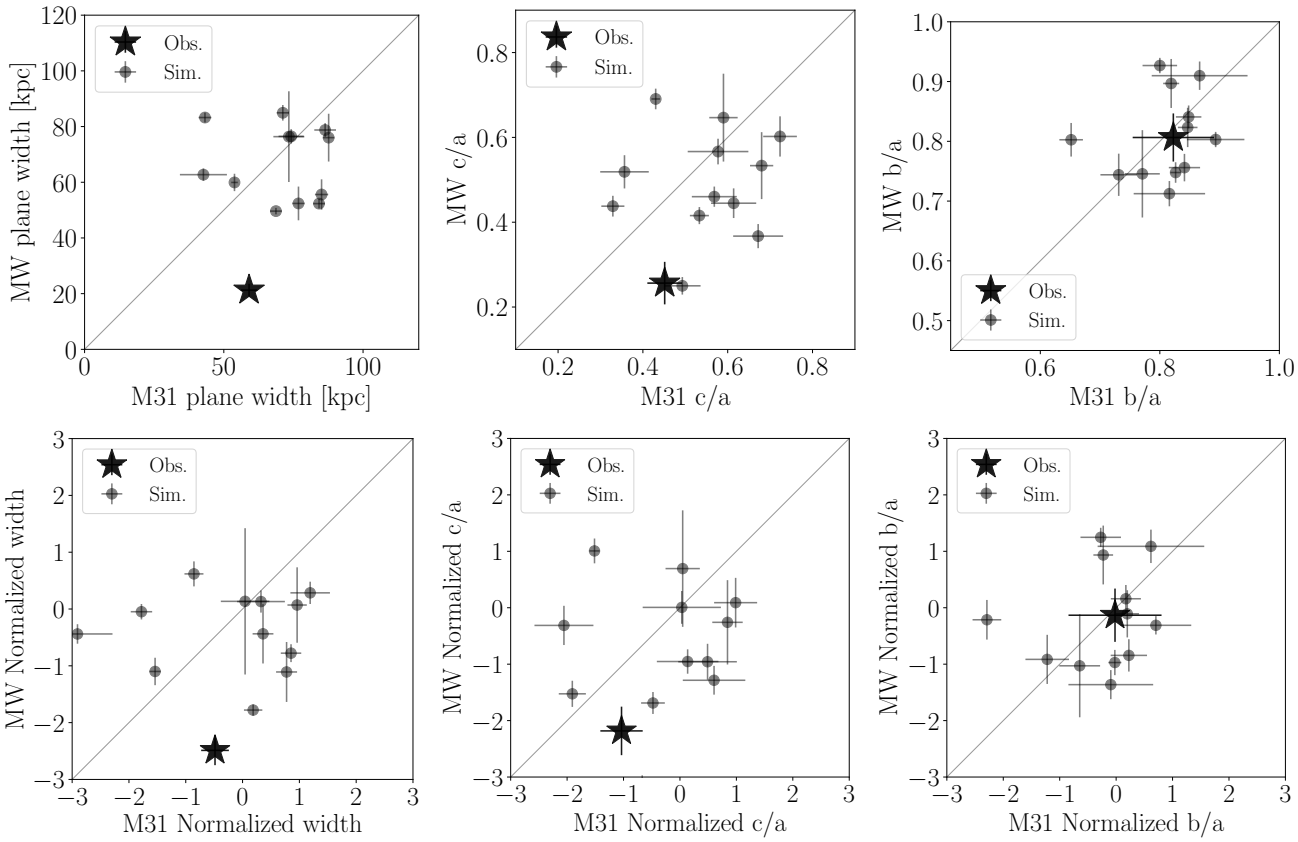

Figure B1. ELVIs results for the quantities presented for the Illustris1-Dark simulation in Figures 1, 2, 3. Upper row corresponds to the raw values from observations and simulated pairs, while the second row normalizes the same values to the mean and standard deviation on its spherically randomized counterparts.

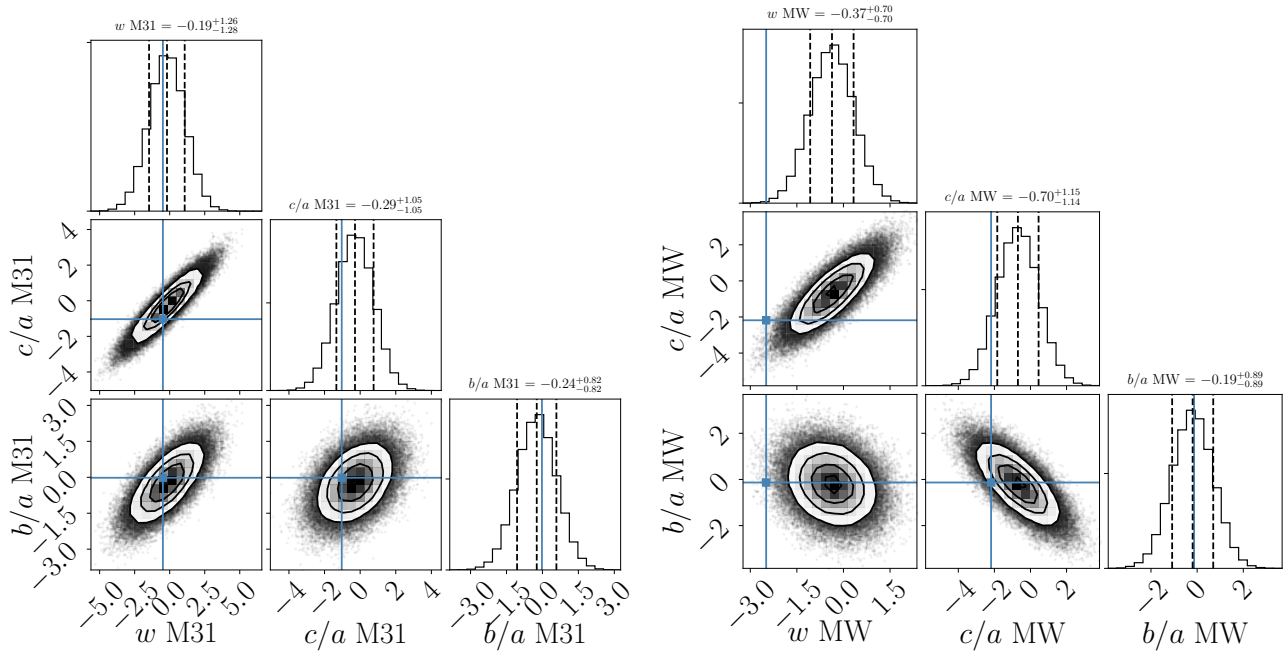

Figure B2. Same layout as Figure 4, this time computed from the ELVIS data.

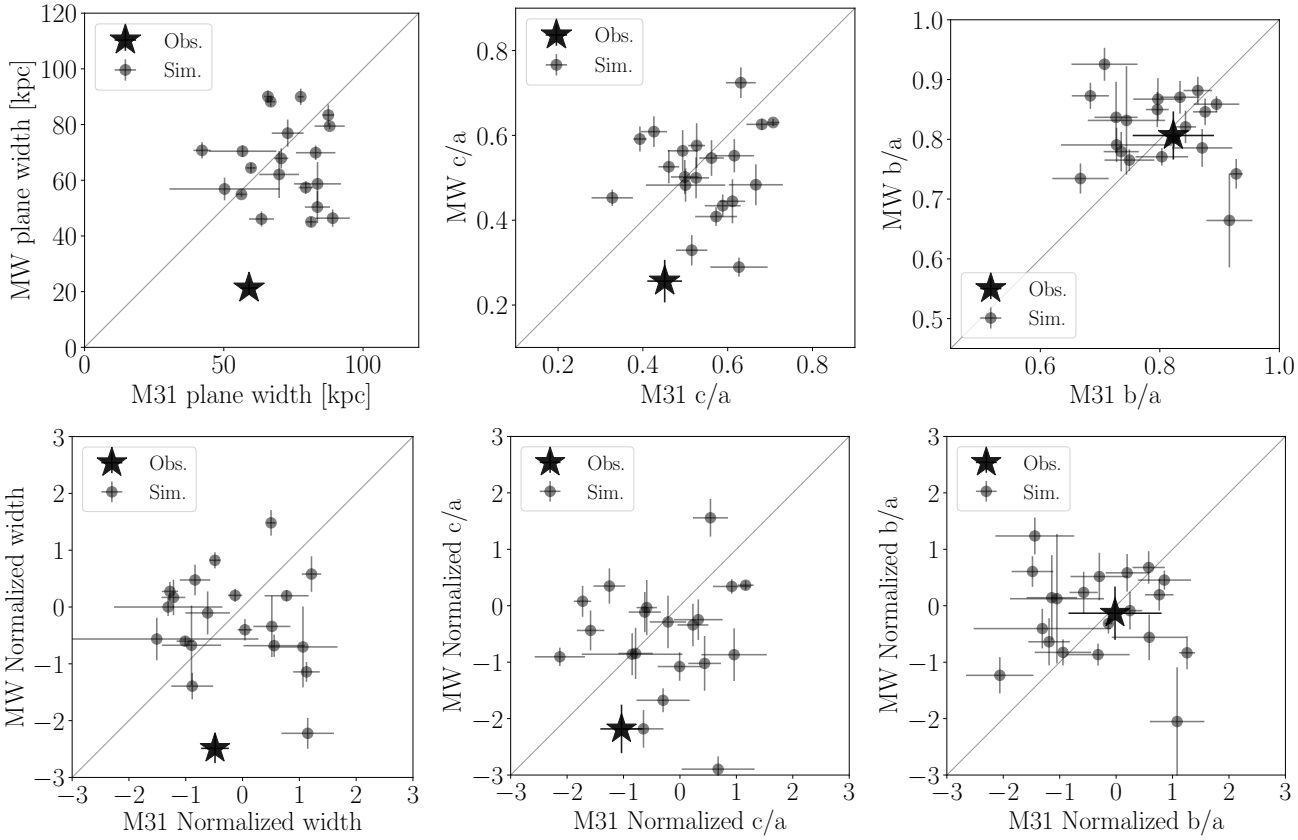

Figure B3. Same layout as Figure B1, this time computed from the Illustris1 data.

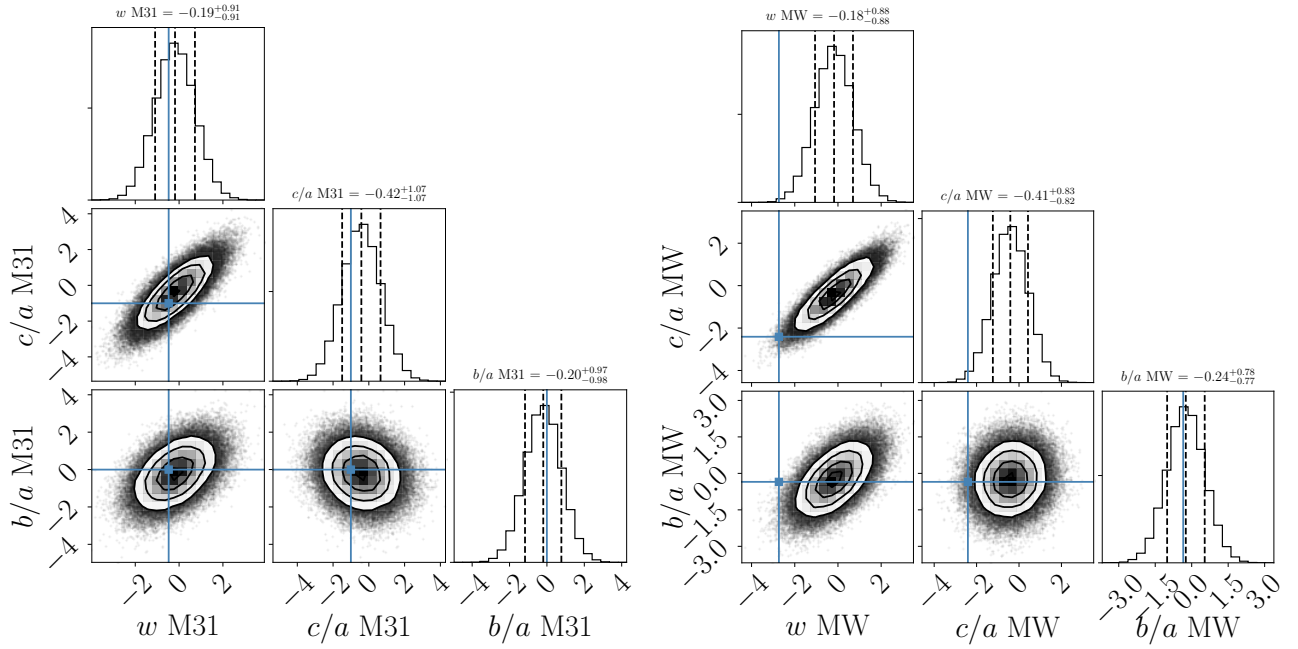

Figure B4. Same layout as Figure 4, this time computed from the Illustris1 data.

APPENDIX C: COVARIANCE MATRICES AND MEAN VALUE VECTORS

C1 Illustris-1

C1.1 M31

$$\Sigma = \begin{bmatrix} 0.83 \pm 0.03 & 0.78 \pm 0.04 & 0.41 \pm 0.04 \\ 0.78 \pm 0.04 & 1.16 \pm 0.05 & -0.15 \pm 0.05 \\ 0.41 \pm 0.04 & -0.15 \pm 0.05 & 0.96 \pm 0.04 \end{bmatrix}$$

$$\mu = \begin{bmatrix} -0.18 \pm 0.04 & -0.41 \pm 0.05 - 0.20 \pm 0.05 \end{bmatrix}$$

C1.2 MW

$$\Sigma = \begin{bmatrix} 0.78 \pm 0.06 & 0.63 \pm 0.07 & 0.40 \pm 0.03 \\ 0.63 \pm 0.07 & 0.69 \pm 0.08 & 0.06 \pm 0.02 \\ 0.40 \pm 0.03 & 0.06 \pm 0.02 & 0.61 \pm 0.04 \end{bmatrix}$$

$$\mu = \begin{bmatrix} -0.17 \pm 0.04 & -0.40 \pm 0.04 - 0.23 \pm 0.04 \end{bmatrix}$$

C2 Illustris-1-Dark

C2.1 M31

$$\Sigma = \begin{bmatrix} 1.50 \pm 0.08 & 1.27 \pm 0.08 & 0.64 \pm 0.04 \\ 1.27 \pm 0.08 & 1.31 \pm 0.08 & 0.28 \pm 0.04 \\ 0.64 \pm 0.04 & 0.28 \pm 0.04 & 0.70 \pm 0.04 \end{bmatrix}$$

$$\mu = \begin{bmatrix} -0.37 \pm 0.05 & -0.55 \pm 0.05 & -0.13 \pm 0.03 \end{bmatrix}$$

C2.2 MW

$$\Sigma = \begin{bmatrix} 1.03 \pm 0.05 & 0.94 \pm 0.05 & 0.36 \pm 0.03 \\ 0.94 \pm 0.05 & 1.24 \pm 0.07 & -0.18 \pm 0.04 \\ 0.36 \pm 0.03 & -0.18 \pm 0.04 & 0.86 \pm 0.03 \end{bmatrix}$$

$$\mu = \begin{bmatrix} -0.45 \pm 0.04 & -0.61 \pm 0.05 & -0.31 \pm 0.04 \end{bmatrix}$$

C3 ELVIS

C3.1 M31

$$\Sigma = \begin{bmatrix} 1.60 \pm 0.19 & 1.22 \pm 0.14 & 0.70 \pm 0.09 \\ 1.22 \pm 0.14 & 1.08 \pm 0.10 & 0.35 \pm 0.05 \\ 0.70 \pm 0.09 & 0.35 \pm 0.05 & 0.63 \pm 0.10 \end{bmatrix}$$

$$\mu = \begin{bmatrix} -0.18 \pm 0.08 & -0.28 \pm 0.07 & -0.22 \pm 0.05 \end{bmatrix}$$

C3.2 MW

$$\Sigma = \begin{bmatrix} 0.45 \pm 0.04 & 0.61 \pm 0.09 & -0.11 \pm 0.09 \\ 0.61 \pm 0.09 & 1.21 \pm 0.17 & -0.63 \pm 0.09 \\ -0.11 \pm 0.05 & -0.63 \pm 0.09 & 0.64 \pm 0.06 \end{bmatrix}$$

$$\mu = \begin{bmatrix} -0.32 \pm 0.04 - 0.74 \pm 0.07 - 0.08 \pm 0.05 \end{bmatrix}$$